analytical chemistry

pubs.acs.org/ac Article

CDMS Analysis of Intact 19S, 20S, 26S, and 30S Proteasomes: Evidence for Higher-Order 20S Assemblies at a Low pH†

Adam J. Anthony, Amit K. S. Gautam, Lohra M. Miller, Yiran Ma, Anya G. Hardwick, Anu Sharma, Subhadip Ghatak, Andreas Matouschek, Martin F. Jarrold, and David E. Clemmer*

Cite This: *Anal. Chem.* 2023, 95, 12209−12215 Read Online

ACCESS | Metrics & More | Article Recommendations | Supporting Information

ABSTRACT: Charge detection mass spectrometry (CDMS) was examined as a means of studying proteasomes. To this end, the following masses of the 20S, 19S, 26S, and 30S proteasomes from *Saccharomyces cerevisiae* (budding yeast) were measured: m(20S) = 738.8 ± 2.9 kDa, m(19S) = 926.2 ± 4.8 kDa, m(26S) = 1,637.0 ± 7.6 kDa, and m(30S) = 2,534.2 ± 10.8 kDa. Under some conditions, larger $(20S)_x$ (where x = 1 to ∼13) assemblies are observed; the 19S regulatory particle also oligomerizes, but to a lesser extent, forming $(19S)_x$ complexes (where x = 1 to 4, favoring the x = 3 trimer). The $(20S)_x$ oligomers are favored in vitro, as the pH of the solution is lowered (from 7.0 to 5.4, in a 20 mM ammonium acetate solution) and may be related to in vivo proteasome storage granules that are observed under carbon starvation. From measurements of $m(20S)_x$ (x = 1 to ∼13) species, it appears that each multimer retains all 28 proteins of the 20S complex subunit. Several types of structures that might explain the formation of $(20S)_x$ assemblies are considered. We stress that each structural type [hypothetical planar, raft-like geometries (where individual proteasomes associate through side-by-side interactions); elongated, rodlike geometries (where subunits are bound end-to-end); and geometries that are roughly spherical (arising from aggregation through nonspecific subunit interactions)] is highly speculative but still interesting to consider, and a short discussion is provided. The utility of CDMS for characterizing proteasomes and related oligomers is discussed.

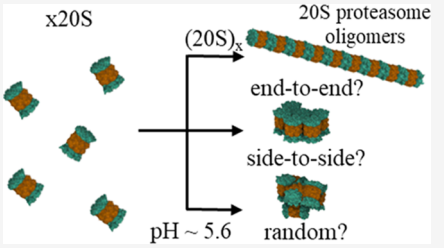

INTRODUCTION

Proteasomes are structurally well-defined biomolecular machines that are involved in regulating the vast majority of cellular processes in eukaryotes through the controlled degradation of proteins.[1,2] Scheme 1 shows a high-resolution cryogenic electron microscopy image along with a schematic diagram illustrating the structure of the 26S proteasome found in *Saccharomyces cerevisiae* (budding yeast), a simple eukaryote. This proteasome is made up of the 19S regulatory particle, composed of 19 individual protein subunits, attached to the end of the 20S core particle, an assembly of 28 proteins arranged in a stack of four, heptameric-protein rings. The open end of the core of the 26S structure can be capped with a second 19S regulatory particle, forming the 30S proteasome (not shown).[3] In the work described below, we examine intact 20S, 19S, as well as 26S and 30S yeast proteasomes and their assembly from core and regulatory particles using a prototype charge detection mass spectrometry (CDMS) technique. In every case, the masses that are derived from CDMS are near several prior MS measurements for these systems.[4−7]

CDMS is particularly useful for characterizing very large protein complexes,[8−10] having masses that extend into the megadalton (MDa) to gigaDa regime—beyond the range of conventional MS measurements.[11,12] While investigating the formation of the larger 26S and 30S proteasomes, we found evidence for several high-mass 19S oligomers, including an abundant 19S trimer, as well as a distribution of multimeric $(20S)_x$ (where x ranges from 1 to ∼13) species, favored in acidified solutions. These larger 20S species appear to have relatively well-defined structures in which all 28 proteins comprising each core complex are entirely conserved for every oligomer size. Such *in vitro* assemblies may be related to early steps in the nucleation of larger 20S proteasome granules, observed during carbon starvation, where the intracellular pH suddenly drops and the 19S and 20S proteasome particles dissociate and are sequestered into proteasome storage granules.[13,14] Cytosolic acidification has also been associated with aging.[15]

Below, we briefly consider several hypothetical higher-order structures that might be adopted by $(20S)_x$ clusters. Overall, these studies illustrate the unique capabilities of CDMS as a means of complementing other techniques for characterizing proteasome expression and sample integrity (purity and structure) as well as facilitating the discovery of higher-order proteasome assemblies. CDMS could also be used to study the

Received: January 31, 2023
Accepted: July 25, 2023
Published: August 8, 2023

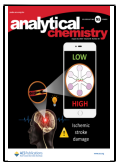

https://doi.org/10.1021/acs.analchem.3c00472
Anal. Chem. 2023, 95, 12209−12215

Scheme 1. Molecular Architecture and Subunit Arrangement of the 26S Proteasome[a]

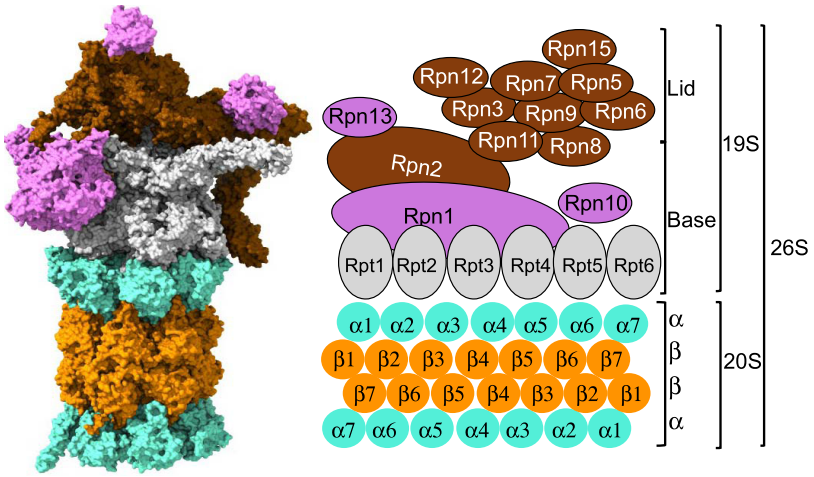

[a]The structure on the left is a three-dimensional rendering of the 26S proteasome (generated by ChimeraX using a 26S structure reported from cryogenic electron microscopy measurements; PDB: 6FVT). The schematic diagram on the right illustrates the positions of individual proteins within the 26S proteasome, which is made up of the 20S core proteasome (a complex of 28 proteins) and the 19S regulatory proteasome (composed of 19 proteins). As can be seen from the structure (left) and schematic (right), the 20S core is an assembly of four stacks of seven-membered rings, referred to as the α- (cyan) and ß-regions (orange). The 19S regulatory proteasome contains six ATPase subunits (Rpt1 to 6) associated with the base subcomplex (gray), non-ATPase subunits (Rpn) in the base, and lid subregions (brown), as well as the ubiquitin receptors (purple).

kinetics of proteasome activity as the machine undergoes conformational changes and hydrolyzes its substrates sequentially. It could be adapted for the study of other macromolecule assemblies and dissecting the role of soluble oligomers of the aggregating protein β-amyloid protein (Aβ) in Alzheimer's disease, α-synuclein in Parkinson's disease, and other pathologies associated with the disruption of proteostasis and the resulting formation of aggregates.

EXPERIMENTAL SECTION

CDMS Measurements. The prototype CDMS instrumentation and measurement protocols used to determine the number (z) of charges (e) and mass-to-charge ratio (m/z) of particles are presented elsewhere.[8] Briefly, nanoelectrospray ionization (n-ESI) is used to transfer biological complexes from solution into the gas phase.[16,17] Ions enter the instrument through a capillary and are focused into a hexapole region before they pass through a hemispherical energy analyzer that is used to select a narrow distribution of ion energies. The energy-selected ions are subsequently introduced into an electrostatic linear ion trap where single ions are analyzed (described previously).[8] For each experimental sequence, a trapped ion oscillates between the trap end-caps, passing back and forth through a charge detection cylinder during each oscillation. The signal induced on the detection cylinder each time the ion passes through is used to determine z for each ion; m/z of each ion is determined from the measured oscillation frequency. A trapping time of 100 ms was used in these studies. Mass spectra are acquired by accumulating many CDMS measurements for individual ions. More details about these measurements, including a schematic diagram of the CDMS instrument, are provided in the SI.

Preparation of Proteasome Samples. 19S, 20S, 26S, and 30S proteasomes were expressed from yeast and purified as described previously.[18,19] The details of the procedures that were used to express and prepare each proteasome sample as well as solutions for n-ESI are provided in the SI.

Measurement Sensitivity and Total Analysis Time. Each experiment was carried out using ~10 μL of sample solution at a concentration of ~10^9 to 10^{10} particles·ml^{-1}. A data acquisition time of ~20 to 30 min was used to analyze each sample. Values of z and m/z for ~4000 ions are acquired under these conditions. See the SI for more information.

RESULTS AND DISCUSSION

Example CDMS spectra for the 20S, 19S, 26S, and 30S proteasomes. Figure 1 shows three example charge versus mass plots that are obtained from an n-ESI-CDMS measurement of isolated 20S and 19S proteasome samples as well as a solution where we mixed these samples (all three samples were analyzed in the presence of 10 μM ATP), to form the 26S and 30S proteasomes. The charge vs mass plots shown in Figure 1 are converted to mass spectra (also shown) by integrating the signals into 5.0 kDa bins across the charge dimension. Typical CDMS mass spectra obtained for the 20S proteasome are dominated by a peak at $m \sim 738.8$ kDa and $e \sim 51$. Inspection of the mass vs charge plots shows that some other ions are dispersed over a broad range of higher m and e values. While these signals correspond to ions that have been trapped and analyzed, they can be thought of as the background (chemical) noise of this measurement, as there is no region of appreciable abundance that appears as a peak.

The 19S proteasome sample shows two peaks: one centered at $m \sim 930$ kDa and $e \sim 63$ corresponding to the 19S regulatory particle and a second unexpected peak at $m \sim 2.5$ MDa and $e \sim 120$, assigned to some remaining 2.5 MDa 30S proteasome impurity. We note that the abundance of this impurity varies depending on the amount of the 20S core proteasome in each sample. In this case, the more abundant 19S proteasome caps both ends of all of the less abundant 20S impurity. From the magnitudes of these peaks, we estimate that the 20S impurity in this preparation makes up ~16% of the sample. When additional 20S proteasome is added to the 19S sample, three peaks are observed: the 19S peak at $m \sim 930$

https://doi.org/10.1021/acs.analchem.3c00472
Anal. Chem. 2023, 95, 12209−12215

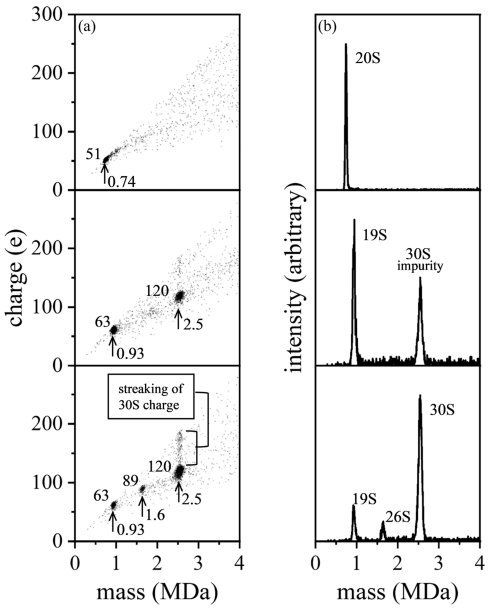

Figure 1. (a) CDMS mass vs charge plots recorded for samples of 20S (top), 19S (middle), and a mixture of these samples that leads to the formation of the 26S and 30S proteasomes (bottom). The arrows indicate the centers of intensity in the charge and mass dimensions. (b) Mass spectra for the 20S (top), 19S (middle), and 26S and 30S proteasomes (bottom) obtained by integrating the signals across the charge dimension into 5 kDa bins.

kDa and $e \sim 63$ (comprising ~13% of the ion intensity); a new smaller peak (~7% of the distribution) at $m \sim 1.6$ MDa and $e \sim 89$ assigned to the 1.6 MDa 26S complex; and a larger peak (~80% of the signal) at $m \sim 2.5$ MDa and $e \sim 120$, assigned as the 30S proteasome.

Two additional aspects of these data are noteworthy. First, the mass peak assigned to the 20S proteasome is substantially narrower than peaks associated with the 19S, 26S, and 30S proteasomes. Such differences imply that the heterogeneities of these proteasome complexes vary. It appears that the 20S core is substantially more homogeneous than the 19S regulatory cap. When the 20S and 19S proteasomes are combined, the larger 26S and 30S species inherit the heterogeneity inherent in the 19S cap. The proteasome is known to be a heterogeneous macromolecule. Apart from various proteasome assembly chaperones, different proteasome interacting proteins (PIP) also contribute to the heterogeneity of assembled proteasomes. Many of these associations are transient and may be nonstoichiometric. Moreover, many proteasomal subunits contain disordered regions, which participate in the regulation of proteasome activity.[20,21] Disordered regions serve as the sites of post-translational modifications or protein−protein interactions.[22,23] Additionally, the structures of the 19S and 20S species may differ in the ease of association of desolvation with ion formation.

It is also interesting to consider the level of charging that is accommodated by the different particles. From the distribution shown in Figure 1, we find that ~9% of 30S proteasome particles accommodate substantially more charge than the main 30S peak (centered at $e \sim 120$), giving rise to the vertical streak that extends to $e \sim 180$. We interpret the streaking as an indication of a small population of 30S particles, each having a somewhat different structure and, thus, accommodating a different number of charges. The 19S regulatory proteasome is intrinsically more dynamic (by design) than the more symmetric assembly of the four-stacked heptameric rings constituting the 20S core and undergoes conformational changes during an ATP hydrolysis cycle, driving substrate protein engagement, unfolding, and translocation.[24] Large structural changes have been observed in the cryo-EM structures of the proteasome, and the majority of this structural heterogeneity is confined to the 19S particle. It is not hard to imagine that the relatively loose packing of protein subunits and flexible loops dangling near the surfaces of the more dynamic 19S structures (as can be seen in Scheme 1) may correspond to a distribution of ionizable structures. Presumably, upon n-ESI, this structural variability leads to accommodation of additional charge without entirely destabilizing the complex through Coulombic interactions. Structural

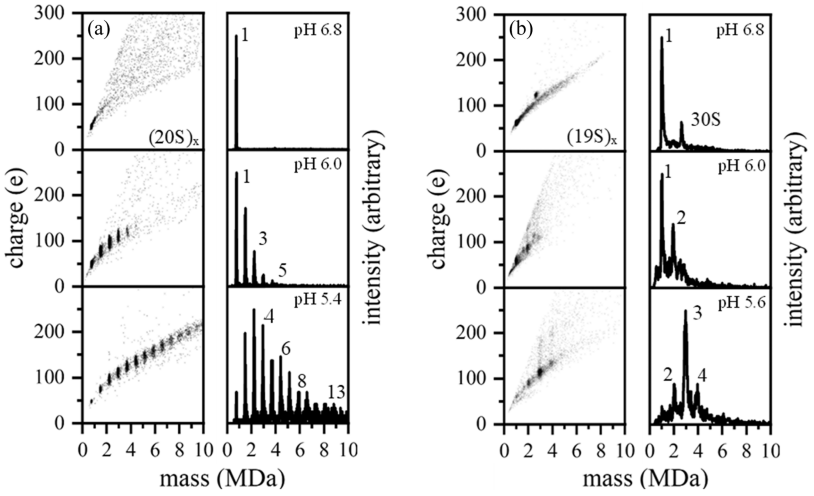

Figure 2. (a) CDMS mass versus charge plots and mass spectra recorded for samples of 20S electrosprayed from 20 mM ammonium acetate solutions at a pH = 6.8 (top), 6.0 (middle), and 5.4 (bottom). As the 20 mM solution is acidified, the 20S proteasome oligomerizes and $(20S)_x$ (x = 1 to 13) over the entire range of pH = 7 to 5.4. At lower pH values, the proteasome and its oligomers disassemble and only species with masses less than the mass of the 20S complex are observed. (b) Analogous study of the 19S proteasome sample. At low pH values $(19S)_x$ (x = 1 to 4), oligomers are observed. The trimer complex appears to be the most stable of the observed oligomers.

https://doi.org/10.1021/acs.analchem.3c00472
Anal. Chem. 2023, 95, 12209−12215

differences that influence particle charging are consistent with the broader mass peaks, as mentioned above.

Evidence for higher-order $(20S)_x$ (x = 1 to 13) and $(19S)_x$ (x = 1 to 4) oligomers. It is interesting to consider the effects of solution pH and ammonium acetate solution concentration on the distributions of species observed in these proteasome samples. While searching for optimal conditions for producing intact proteasome ions (which appears to be in solutions of ∼100 to 200 mM ammonium acetate, near pH = 7), we found evidence for oligomerization of 20S proteasomes upon decreasing the pH in low-solution-concentration solutions. Figure 2 shows an example of typical data obtained in 20 mM ammonium acetate at pH = 6.8, 6.0, and 5.4 (additional pH values are shown in the SI). From pH = 7 to ∼6, small oligomers of $(20S)_x$ (where x = 1 to 5) are observed. As we continue to acidify the solution, further oligomerization to a maximum of ∼13 20S subunits is detected. Interestingly, charge streaking is not observed for $(20S)_x$ species. Instead, the range of charges associated with each oligomer size is relatively well conserved (± ∼ 10 for each), suggesting that these species may be assembling into well-defined structures. Below pH = 5.4, the sample appears to decompose such that no peaks as large as the 20S monomer are observed. Presumably, at a low pH, the 20S oligomers are no longer stable, and the structure disassembles, resulting in smaller fragments (not shown). A similar study of the 19S proteasome showed that this particle is far less prone to oligomerization. As also shown in Figure 2, over a range of solution conditions, we do observe x = 1 to 4 $(19S)_x$ oligomers; however, the 19S trimer appears to be most stable.

CDMS masses for the intact 20S, 19S, 26S, and 30S proteasomes. A summary of masses from replicate measurements for the 20, 19, 26, and 30S proteasomes obtained from CDMS is provided in Table 1. In the Supporting Information, we include the theoretical masses for individual proteins that were used to obtain the theoretical values for the intact species. These data are obtained by averaging the peak centers of independent measurements determined from a Gaussian fit to each peak. From five measurements for the 20S and 19S proteasomes, we find average values of $m(20S)$ = 738.8 ± 2.9 and $m(19S)$ = 926.2 ± 4.8 kDa. Four measurements were obtained for the 26S proteasome, yielding an average of $m(26S)$ = 1637.0 ± 7.6 kDa, 28.0 kDa less than the sum of masses of 1665.0 ± 5.6 kDa measured for the 20S and 19S proteasomes. Ten measurements were acquired for the 30S proteasome, yielding an average of $m(30S)$ = 2534.2 ± 10.8 kDa, a value that is 57.0 kDa less than the 2591.2 ± 7.7 kDa mass predicted upon combining our experimental measurements for the 20S core with two 19S caps. A summary of these measurements is provided in Table 1.

Table 1. Comparison of CDMS Masses for Yeast Proteasomes with Prior Measurements

reported by	m20S (?)[a]	m19S (?)	m26S (?)	m30S (?)
Robinson[b]	746.0 (0.1)	na	1658.4 (0.3)	2587.4 (0.4)
expected	727.7	928.9	1656.6	2585.5
Sharon[c]	731.2 (0.2)	na	na	na
expected	730.7			
CDMS[d]	738.8 (2.9)	926.2 (4.8)	1637.0 (7.6)	2534.2 (10.8)
expected	734.9	928.7	1663.6	2592.3

[a]All masses are reported in kDa and correspond to the mean value from multiple measurements of proteasomes expressed from yeast. Uncertainties (σ) are provided in parentheses and correspond to one standard deviation. [b]Measured masses for the 20S, 26S, and 30S proteasomes by Robinson and co-workers from ref 4. A value for the expected mass of each proteasome is reported directly below the average measured mass. Expected values are calculated from the masses of individual proteins in each complex. We note that some ambiguity (variation) in these values arises because the degree of postexpression processing (i.e., autocleavages and post-translational modifications) is not well defined. An indication of "na" implies that this value was not available (i.e., not reported). [c]Measured mass of the 20S proteasome determined by Sharon and co-workers from ref 6. The expected mass calculated for this proteasome is provided below the measured value. [d]Measured masses of the 19S, 20S, 26S, and 30S proteasomes determined in the present study by CDMS. Expected masses that are calculated for each proteasome are provided below each measured value.

Evidence that $(20S)_x$ (x = 1 to 13) oligomers are composed of intact 20S complexes. It is interesting to examine the masses of each $(20S)_x$ oligomer in more detail. This provides a means of assessing the integrity of the 20S subunits within each multimer size. That is, are all 28 substituent proteins within the 20S complex retained in each oligomerized form? Figure 3 shows a plot of the average masses for each of the $(20S)_x$ oligomers. From the slope of a linear fit to these values, we see that the average mass increase (associated with adding a single 20S monomer to each multimer size) is $m(20S)$ = 731.4 ± 8.4 kDa. This determination of $m(20S)$ is in agreement with $m(20S)$ = 738.8 ± 2.9 kDa, measured directly for the 20S monomer (Table 1). Insight into the integrity of the individual 20S subunits is obtained by examining the differences between adjacent multimers [i.e., $m(20S)_x - m(20S)_{x-1}$ for x = 2 to 11 considered in these studies]. These differences in mass are also indicated in Figure 3. In each case, the mass difference of adjacent multimers is consistent with what is expected for the addition of the 20S monomer. From the masses for the individual 20S proteins (Table SII), we calculate masses of

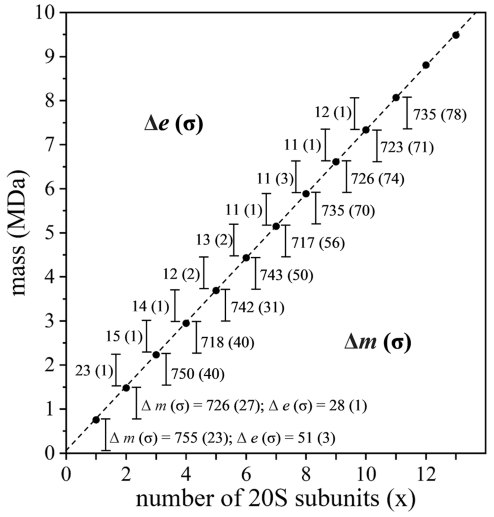

Figure 3. Average changes in mass (kDa) and charge (e) with respective standard deviations upon addition of a single 20S monomer to any given multimer size are shown. A fit to the line for the measured data points at each oligomer size is given by the following equation: $y = (731.4 \pm 8.4)x + (28.6)$. The y-intercept is likely above zero due to the low salt concentration used for these studies which may form species that are not fully desolvated.

https://doi.org/10.1021/acs.analchem.3c00472
Anal. Chem. 2023, 95, 12209−12215

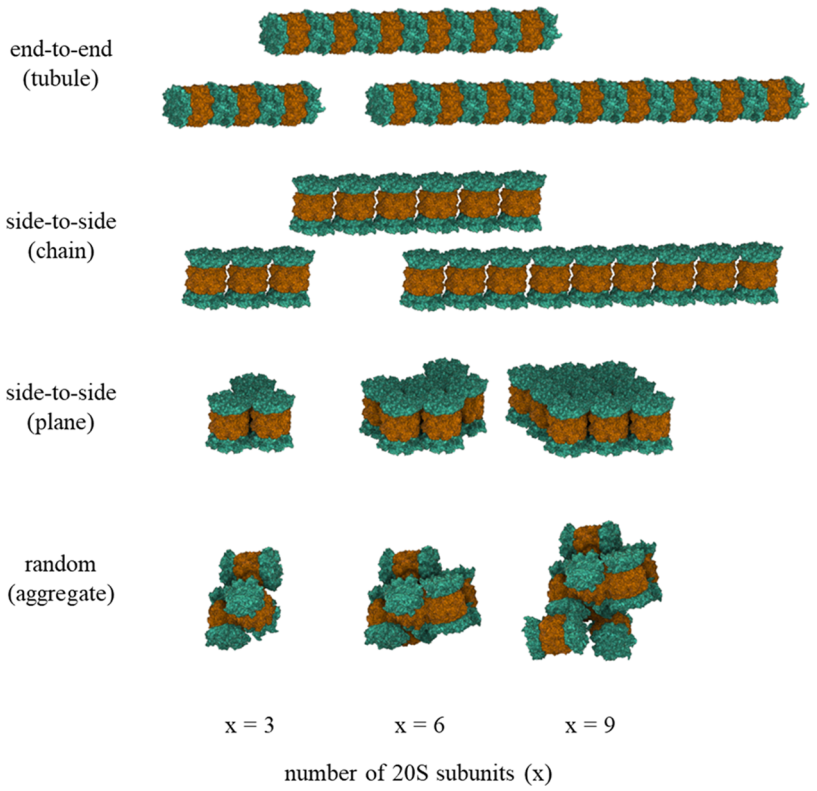

Figure 4. Four multimer models for the 20S core are presented: end-to-end (chain), side-to-side (chain), side-to-side (plane), and random (aggregate). For each model, three theoretical multimer sizes are shown (x = 3, 6, and 9). While either end-to-end or random formation of the 20S proteasome may reduce functional ability, a side-to-side model allows for the 20S complex to retain access to the entrance of the α ring.

~198 and ~170 kDa for the seven-membered α- and ß-rings, respectively (also provided in Table SII). The mass uncertainties determined for multimers are much less (~10 to 70 kDa). From this, we conclude that no seven-membered protein rings are missing for any multimer sizes. It is more difficult to rule out the loss of a single individual protein for all multimers. The masses of the 14 unique proteins (Table SII) in the 20S proteasome ranging from ~21.5 to ~31.5 kDa are such that we cannot unambiguously rule out the loss of a single protein for all multimer sizes. However, because the masses of the differently sized multimers remain centered near a multiple of the measured mass of the 20S monomer (738.8 ± 2.9 kDa), the deletion of any single protein within the 20S multimers seems unlikely, and it is difficult to imagine structures that accommodate smaller individual rings in the particles.

Structural considerations for $(20S)_x$ multimers. We cannot resist speculating about possible structures for $(20S)_x$ multimers. It is important to stress that these are hypothetical structural types and are intended only as suggestions of how 20S might oligomerize. That we find no evidence for loss of protein monomers or rings suggests that the 20S core can be treated as an intact subunit as it assembles to form higher-order multimers. As noted above, we interpret the relatively tight and similar range of charges observed for each multimer size as an indication that 20S monomers may be associating together, forming an ordered (or somewhat ordered) assembly. With this in mind, we suggest three probable configurations of subunit association: one in which the 20S subunits are bound end-to-end through interactions of the α rings; another where association of subunits occurs through side-to-side interactions; and finally, association through random (nonspecific) interactions. Figure 4 shows several hypothetical structural types (for the x = 3, 6, and 9 multimers) that would emerge from these binding considerations. End-to-end associations of 20S subunits through contacts between α rings would lead to extended chain-like tubules. One might think of this as assembling the 20S monomer machinery in series. This is a fascinating structure. The crystal structure of the 20S monomer indicates that it has a diameter of ~11 nm and that the stack of four rings has a height of ~15 nm. End-to-end assembly of three particles would yield an ~45 nm long tubule. As additional monomers are included, this type of tubule is expected to become very long, ~ 90 and ~135 nm for the x = 6 and 9 examples shown in Figure 4. One imagines that extended tubular assemblies could be capped at one or both ends with a 19S regulatory particle such that long tubules might retain some ability to degrade proteins, albeit with reduced efficiency.

Side-to-side associations of core particles would lead to chains or planes of 20S subunits, also illustrated as hypothetical structures shown in Figure 4. One might think of this as assembling the 20S monomer machinery in parallel to form proteasome arrays. These structures are also fascinating. Either side of each 20S unit could be capped with a 19S regulatory proteasome. From a functional standpoint, such a dense packing of 20S cores with accessible ends would be expected to be highly efficient. Finally, Figure 4 also shows x = 3, 6, and 9 multimers that have been formed through random associations of particles. This type of mechanism of formation is expected to lead to roughly spherical aggregates.

As suggested, charge may provide additional clues about structure.[25] Because this discussion is so highly speculative, and the use of charge to discriminate between structural types is not established (and also not the focus of this work), we

https://doi.org/10.1021/acs.analchem.3c00472
Anal. Chem. 2023, 95, 12209−12215

present a brief discussion of how the total charge might change as oligomers grow; however, we do not draw any conclusions about structures from these ideas. Briefly, Figure 3 also includes the charge differences between adjacent multimers [i.e., $e(20S)_x - e(20S)_{x-1}$ for $x = 2$ to 11]. As noted, the average charge (obtained by fitting multiple data sets as described for the determination of average mass) carried by the 20S monomer is 51 ± 3e. Upon dimerization, 28 ± 1 additional charges are added (a total of $e(20S)_2 = 79 \pm 2$). Presumably, the charge on the dimer is not twice that of the monomer because some charge-carrying sites are blocked at the interface for binding the two monomers. Upon formation of the trimer, ∼23 ± 1 additional charges are added, measurably smaller than the 28 charge increase upon forming the dimer. Even fewer additional charges are incorporated upon the addition of a fourth (∼15) and then a fifth (∼14) subunit to form the tetramer and pentamer, respectively; beyond this size, each additional 20S subunit increases the total charge by 12 ± 1e. These types of considerations may prove useful in characterizing structural types, especially if paired with other, well-established techniques, such as electron microscopy. While we have initiated these studies, it would be premature to draw conclusions about the relationship between charging and imaging here.

SUMMARY AND CONCLUSIONS

We examined the use of CDMS as a means of characterizing proteasomes. Of particular interest are the masses determined from this study: $m(20S)$ = 738.8 ± 2.9 kDa, $m(19S)$ = 926.2 ± 4.8 kDa, $m(26S)$ = 1,637.0 ± 7.6 kDa, and $m(30S)$ = 2,534.2 ± 10.8 kDa. The measured masses for each of these proteasomes are in good agreement with the prior values reported from conventional MS measurements. Examination of peak shapes in the mass spectra suggests that the structures of 20S core particles are more homogeneous than 19S regulatory proteasomes. Independent measurement of the charge distributions associated with these particles corroborates this idea. Upon mixing, 20S and 19S solutions are mixed, the 26S and 30S proteasomes are formed, and it appears that these products inherit the heterogeneity of the 19S precursor. In acidified, low-buffer-concentration solutions, 20S core particles associate to form higher-order multimers, $(20S)_x$ (where x = 1 to ∼13). The 19S regulatory particle also oligomerizes, but to a lesser extent, forming $(19S)_x$ complexes (where x = 1 to 4, favoring the x = 3 trimer). The measured $(20S)_x$ oligomer masses indicate that the 20S core retains all 28 of its constituent proteins for every oligomer size. We have used the idea that the 20S core remains intact and thus can be thought of as an oligomer subunit, combined with variations associated with the increase in charge upon inclusion of additional subunits as assemblies grow to speculate about possible structures.

ASSOCIATED CONTENT

Supporting Information

The Supporting Information is available free of charge at https://pubs.acs.org/doi/10.1021/acs.analchem.3c00472.

Conversion for ion frequency to m/z measurement (Equation S1); instrument schematic of prototype charge detection mass spectrometer (Figure S1); theoretical mass calculation of 19S proteasome (Table S1); theoretical mass calculation for the 20S proteasome (Table S2); numerical comparison between manual and gaussian peak fits for CDMS peak centers (Table S3); visual comparison between manual and gaussian peak fits for CDMS peak centers (Figure S2); and representative 20S proteasome spectra from pH 7.0 to 5.4 in 0.2 increments (Figure S3) (PDF)

AUTHOR INFORMATION

Corresponding Author

David E. Clemmer − *Department of Chemistry, Indiana University, Bloomington, Indiana 47401, United States;* orcid.org/0000-0003-4039-1360; Email: clemmer@indiana.edu

Authors

Adam J. Anthony − *Department of Chemistry, Indiana University, Bloomington, Indiana 47401, United States*

Amit K. S. Gautam − *Department of Molecular Biosciences, University of Texas, Austin, Texas 78712, United States*

Lohra M. Miller − *Department of Chemistry, Indiana University, Bloomington, Indiana 47401, United States*

Yiran Ma − *Department of Chemistry, Indiana University, Bloomington, Indiana 47401, United States*

Anya G. Hardwick − *Department of Chemistry, Indiana University, Bloomington, Indiana 47401, United States*

Anu Sharma − *Indiana Center for Regenerative Medicine & Engineering, Department of Surgery, Indiana University School of Medicine, Indianapolis, Indiana 46202, United States*

Subhadip Ghatak − *Indiana Center for Regenerative Medicine & Engineering, Department of Surgery, Indiana University School of Medicine, Indianapolis, Indiana 46202, United States;* orcid.org/0000-0001-5641-3902

Andreas Matouschek − *Department of Molecular Biosciences, University of Texas, Austin, Texas 78712, United States;* orcid.org/0000-0001-6016-2341

Martin F. Jarrold − *Department of Chemistry, Indiana University, Bloomington, Indiana 47401, United States;* orcid.org/0000-0001-7084-176X

Complete contact information is available at: https://pubs.acs.org/10.1021/acs.analchem.3c00472

Notes

The authors declare the following competing financial interest(s): The authors declare the following financial conflicts of interest. MFJ and DEC are associated with Megadalton Solutions, a startup company developing charge detection mass spectrometry. All of the other authors declare no competing financial conflicts of interest.

ACKNOWLEDGMENTS

This work was supported in part by grants from the National Institutes of Health R01 GM131100, R01 GM135246-03, R56DK129592, The Welch Foundation (F-1817), and the National Science Foundation CHE-1904749.

DEDICATION

†The authors dedicate this paper to our late colleague James P. Reilly (August 29, 1950 − February 13, 2022). Jim was like the North Star. You could guide your ship by him.

REFERENCES

(1) Bochtler, M.; Ditzel, L.; Groll, M.; Hartmann, C.; Huber, R. *Annu. Rev. Biophys. Biomol. Struct.* **1999**, *28*, 295−317.
(2) Davis, C.; Spaller, B. L.; Matouschek, A. *Curr. Opin. Struct. Biol.* **2021**, *67*, 161−169.
(3) Tanaka, K. *Proc. Jpn. Acad., Ser. B* **2009**, *85* (1), 12−36.
(4) Sakata, E.; Stengel, F.; Fukunaga, K.; Zhou, M.; Saeki, Y.; Forster, F.; Baumeister, W.; Tanaka, K.; Robinson, C. V. *Mol. Cell* **2011**, *42* (5), 637−649.
(5) Sharon, M.; Witt, S.; Felderer, K.; Rockel, B.; Baumeister, W.; Robinson, C. V. *J. Biol. Chem.* **2006**, *281* (14), 9569−9575.
(6) Vimer, S.; Ben-Nissan, G.; Morgenstern, D.; Kumar-Deshmukh, F.; Polkinghorn, C.; Quintyn, R. S.; Vasil'ev, Y. V.; Beckman, J. S.; Elad, N.; Wysocki, V. H.; Sharon, M. *ACS Cent. Sci.* **2020**, *6* (4), 573−588.
(7) Ben-Nissan, G.; Vimer, S.; Tarnavsky, M.; Sharon, M. *Methods Enzymol.* **2019**, *619*, 179−223.
(8) Contino, N. C.; Jarrold, M. F. *Int. J. Mass Spectrom.* **2013**, *345*−*347*, 153−159.
(9) Brown, B. A.; Zeng, X.; Todd, A. R.; Barnes, L. F.; Winstone, J. M. A.; Trinidad, J. C.; Novotny, M. V.; Jarrold, M. F.; Clemmer, D. E. *Anal. Chem.* **2020**, *92* (4), 3285−3292.
(10) Bischoff, A. J.; Harper, C. C.; Williams, E. R.; Francis, M. B. *J. Am. Chem. Soc.* **2022**, *144* (51), 23368−23378.
(11) Brown, B. A.; Guda, P. R.; Zeng, X.; Anthony, A.; Couse, A.; Barnes, L. F.; Sharon, E. M.; Trinidad, J. C.; Sen, C. K.; Jarrold, M. F.; Ghatak, S.; Clemmer, D. E. *Anal. Chem.* **2022**, *94* (25), 8909−8918.
(12) Miller, Lohra M.; Jarrold; Martin, F. *Essays Biochem.* **2022**, *67*, 315−323, DOI: 10.1042/ebc20220101.
(13) Laporte, D.; Salin, B.; Daignan-Fornier, B.; Sagot, I. *J. Cell Biol.* **2008**, *181* (5), 737−745.
(14) Peters, L. Z.; Hazan, R.; Breker, M.; Schuldiner, M.; Ben-Aroya, S. *J. Cell Biol.* **2013**, *201* (5), 663−671.
(15) Knieß, R. A.; Mayer, M. P. *npj Aging Mech. Dis.* **2016**, *2*, No. 16028, DOI: 10.1038/npjamd.2016.28.
(16) Fenn, J. B. *J. Am. Soc. Mass Spectrom.* **1993**, *4* (7), 524−535.
(17) Fenn, J. B.; Mann, M.; Meng, C. K.; Wong, S. F.; Whitehouse, C. M. *Science* **1989**, *246* (4926), 64−71.
(18) Sone, T.; Saeki, Y.; Toh-e, A.; Yokosawa, H. *J. Biol. Chem.* **2004**, *279* (27), 28807−28816.
(19) Gautam, A. K. S.; Martinez-Fonts, K.; Matouschek, A. *Methods Mol. Biol.* **2018**, *1844*, 321−341.
(20) Aufderheide, A.; Unverdorben, P.; Baumeister, W.; Forster, F. *FEBS Lett.* **2015**, *589* (19), 2552−2560.
(21) Gautam, A. K. S.; Yu, H.; Yellman, C.; Elcock, A. H.; Matouschek, A. *Protein Sci.* **2022**, *31* (3), 556−567.
(22) Finley, D.; Prado, M. A. *Cold Spring Harbor Perspect. Biol.* **2020**, *12* (1), No. a033985, DOI: 10.1101/cshperspect.a033985.
(23) Hirano, H.; Kimura, Y.; Kimura, A. *J. Proteomics* **2016**, *134*, 37−46.
(24) Martinez-Fonts, K.; Davis, C.; Tomita, T.; Elsasser, S.; Nager, A. R.; Shi, Y.; Finley, D.; Matouschek, A. *Nat. Commun.* **2020**, *11* (1), No. 477.
(25) Barnes, L. F.; Draper, B. E.; Jarrold, M. F. *Mol. Ther.–Methods Clin. Dev.* **2022**, *27*, 327−336.

https://doi.org/10.1021/acs.analchem.3c00472
Anal. Chem. 2023, 95, 12209−12215